Biomedical Optics EXPRESS

Handheld imaging photonic crystal biosensor for multiplexed, label-free protein detection

Sabrina Jahns,[1,*] Marion Bräu,[2] Björn-Ole Meyer,[1] Torben Karrock,[1] Sören B. Gutekunst,[3] Lars Blohm,[4] Christine Selhuber-Unkel,[3] Raymund Buhmann,[2] Yousef Nazirizadeh,[1] and Martina Gerken[1]

[1]*Institute of Electrical and Information Engineering, Christian-Albrechts-Universität zu Kiel, Germany*
[2]*Department of Medicine III and Transfusion Medicine, University Hospital Grosshadern, LMU, Munich, Germany*
[3]*Institute for Materials Science, Christian-Albrechts-Universität zu Kiel, Germany*
[4]*Biotechnical Microsystems, Fraunhofer Institute of Silicon Technology, Germany*
[*]*sja@tf.uni-kiel.de*

Abstract: We present a handheld biosensor system for the label-free and specific multiplexed detection of several biomarkers employing a spectrometer-free imaging measurement system. A photonic crystal surface functionalized with multiple specific ligands forms the optical transducer. The photonic crystal slab is fabricated on a glass substrate by replicating a periodic grating master stamp with a period of 370 nm into a photoresist via nanoimprint lithography and deposition of a 70-nm titanium dioxide layer. Capture molecules are coupled covalently and drop-wise to the photonic crystal surface. With a simple camera and imaging optics the surface-normal transmission is detected. In the transmission spectrum guided-mode resonances are observed that shift due to protein binding. This shift is observed as an intensity change in the green color channel of the camera. Non-functionalized image sections are used for continuous elimination of background drift. In a first experiment we demonstrate the specific and time-resolved detection of 90.0 nM CD40 ligand antibody, 90.0 nM EGF antibody, and 500 nM streptavidin in parallel on one sensor chip. In a second experiment, aptamers with two different spacer lengths are used as receptor. The binding kinetics with association and dissociation of 250 nM thrombin and regeneration of the sensor surface with acidic tris-HCl-buffer (pH 5.0) is presented for two measurement cycles.

OCIS codes: (280.4788) Optical sensing and sensors; (170.0170) Medical optics and biotechnology; (350.4238) Nanophotonics and photonic crystals; (110.2970) Image detection systems; (220.4241) Nanostructure fabrication.

References and links

1. J. McCord, R. M. Nowak, P. A. McCullough, C. Foreback, S. Borzak, G. Tokarski, M. C. Tomlanovich, G. Jacobsen, and W. D. Weaver, "Ninety-Minute Exclusion of Acute Myocardial Infarction By Use of Quantitative Point-of-Care Testing of Myoglobin and Troponin I," Circulation **104**(13), 1483–1488 (2001).
2. M. B. Schulze, K. Hoffmann, H. Boeing, J. Linseisen, S. Rohrmann, M. Möhlig, A. F. H. Pfeiffer, J. Spranger, C. Thamer, H.-U. Häring, A. Fritsche, and H.-G. Joost, "An Accurate Risk Score based on Anthropometric, Dietary, and Lifestyle Factors to Predict the Development of Type 2 Diabetes," Diabetes Care **30**(3), 510–515 (2007).
3. F. Wei, P. Patel, W. Liao, K. Chaudhry, L. Zhang, M. Arellano-Garcia, S. Hu, D. Elashoff, H. Zhou, S. Shukla, F. Shah, C.-M. Ho, and D. T. Wong, "Electrochemical Sensor for Multiplex Biomarkers Detection," Clin. Cancer Res. **15**(13), 4446–4452 (2009).
4. C.-S. Huang, V. Chaudhery, A. Pokhriyal, S. George, J. Polans, M. Lu, R. Tan, R. C. Zangar, and B. T. Cunningham, "Multiplexed Cancer Biomarker Detection Using Quartz-based Photonic Crystal Surfaces," Anal. Chem. **84**(2), 1126–1133 (2012).
5. O. Bleher, A. Schindler, M.-X. Yin, A. B. Holmes, P. B. Luppa, G. Gauglitz, and G. Proll, "Development of a new parallelized, optical biosensor platform for label-free detection of autoimmunity-related antibodies," Anal. Bioanal. Chem. **406**(14), 3305–3314 (2014).

#246022 Received 14 Jul 2015; revised 14 Aug 2015; accepted 14 Aug 2015; published 1 Sep 2015

6. L. Römhildt, C. Pahlke, F. Zörgiebel, H.-G. Braun, J. Opitz, L. Baraban, and G. Cuniberti, "Patterned Biochemical Functionalization Improves Aptamer-Based Detection of Unlabeled Thrombin in a Sandwich Assay," ACS Appl. Mater. Interfaces **5**(22), 12029–12035 (2013).
7. P. Kozma, F. Kehl, E. Ehrentreich-Förster, C. Stamm, and F. F. Bier, "Integrated planar optical waveguide interferometer biosensors: a comparative review," Biosens. Bioelectron. **58**, 287–307 (2014).
8. H.-M. Haake, A. Schütz, and G. Gauglitz, "Label-free detection of biomolecular interaction by optical sensors," Fresenius J. Anal. Chem. **366**(6-7), 576–585 (2000).
9. H. Nakamura and I. Karube, "Current research activity in biosensors," Anal. Bioanal. Chem. **377**(3), 446–468 (2003).
10. X. Fan, I. M. White, S. I. Shopova, H. Zhu, J. D. Suter, and Y. Sun, "Sensitive optical biosensors for unlabeled targets: A review," Anal. Chim. Acta **620**(1-2), 8–26 (2008).
11. C. L. Wong and M. Olivo, "Surface Plasmon Resonance Imaging Sensors: A Review," Plasmonics **9**(4), 809–824 (2014).
12. R. Bruck, E. Melnik, P. Muellner, R. Hainberger, and M. Lämmerhofer, "Integrated polymer-based Mach-Zehnder interferometer label-free streptavidin biosensor compatible with injection molding," Biosens. Bioelectron. **26**(9), 3832–3837 (2011).
13. W. Peng, Y. Liu, P. Fang, X. Liu, Z. Gong, H. Wang, and F. Cheng, "Compact surface plasmon resonance imaging sensing system based on general optoelectronic components," Opt. Express **22**(5), 6174–6185 (2014).
14. H. K. Hunt and A. M. Armani, "Bioconjugation strategies for label-free optical microcavity sensors," IEEE J. Sel. Top. Quantum Electron. **20**(2), 6900213 (2014).
15. R. D. Peterson, B. T. Cunningham, and J. E. Andrade, "A photonic crystal biosensor assay for ferritin utilizing iron-oxide nanoparticles," Biosens. Bioelectron. **56**, 320–327 (2014).
16. S.-F. Lin, T.-J. Ding, J.-T. Liu, C.-C. Lee, T.-H. Yang, W.-Y. Chen, and J.-Y. Chang, "A Guided Mode Resonance Aptasensor for Thrombin Detection," Sensors (Basel) **11**(12), 8953–8965 (2011).
17. D. Threm, Y. Nazirizadeh, and M. Gerken, "Photonic Crystal Biosensors Towards On-Chip Integration," J. Biophotonics **5**(8-9), 601–616 (2012).
18. B. Zhang, A. W. Morales, R. Peterson, L. Tang, and J. Y. Ye, "Label-free detection of cardiac troponin I with a photonic crystal biosensor," Biosens. Bioelectron. **58**, 107–113 (2014).
19. G. Y. Song, W. J. Kim, H. Ko, B. K. Kim, K. H. Kim, C. Huh, and J. Hong, "Portable guided-mode resonance biosensor platform for point-of-care testing," Proc. SPIE **84600**, 84600F (2012).
20. D. Gallegos, K. D. Long, H. Yu, P. P. Clark, Y. Lin, S. George, P. Nath, and B. T. Cunningham, "Label-free biodetection using a smartphone," Lab Chip **13**(11), 2124–2132 (2013).
21. A. E. Cetin, A. F. Coskun, B. C. Galarreta, M. Huang, D. Herman, A. Ozcan, and H. Altug, "Handheld high-throughput plasmonic biosensor using computational on-chip imaging," Light Sci. Appl. **3**(1), 1–10 (2014).
22. S. Fan and J. D. Joannopoulos, "Analysis of guided resonances in photonic crystal slabs," Phys. Rev. B **65**(23), 235112 (2002).
23. Y. Nazirizadeh, J. Reverey, U. Geyer, U. Lemmer, C. Selhuber-Unkel, and M. Gerken, "Material-based three-dimensional imaging with nanostructured surfaces," Appl. Phys. Lett. **102**(1), 011116 (2013).
24. Y. Zhuo, H. Hu, W. Chen, M. Lu, L. Tian, H. Yu, K. D. Long, E. Chow, W. P. King, S. Singamaneni, and B. T. Cunningham, "Single nanoparticle detection using photonic crystal enhanced microscopy," Analyst (Lond.) **139**(5), 1007–1015 (2014).
25. Y. Nazirizadeh, U. Bog, S. Sekula, T. Mappes, U. Lemmer, and M. Gerken, "Low-cost label-free biosensors using photonic crystals embedded between crossed polarizers," Opt. Express **18**(18), 19120–19128 (2010).
26. S. Jahns, P. Glorius, M. Hansen, Y. Nazirizadeh, and M. Gerken, "Imaging label-free biosensor with microfluidic system,"Bio-MEMS and Medical Devices II Proc. of SPIE **9518** (2015).
27. D. M. Tasset, M. F. Kubik, and W. Steiner, "Oligonucleotide inhibitors of human thrombin that bind distinct epitopes," J. Mol. Biol. **272**(5), 688–698 (1997).
28. S. Song, L. Wang, J. Li, J. Zhao, and C. Fan, "Aptamer-based biosensors," TrAC **27**, 107–117 (2008).
29. J. A. Kolberg, T. Jørgensen, R. W. Gerwien, S. Hamren, M. P. McKenna, E. Moler, M. W. Rowe, M. S. Urdea, X. M. Xu, T. Hansen, O. Pedersen, and K. Borch-Johnsen, "Development of a type 2 diabetes risk model from a panel of serum biomarkers from the Inter99 cohort," Diabetes Care **32**(7), 1207–1212 (2009).
30. C. A. Meier, E. Bobbioni, C. Gabay, F. Assimacopoulos-Jeannet, A. Golay, and J.-M. Dayer, "IL-1 Receptor Antagonist Serum Levels Are Increased in Human Obesity: A Possible Link to the Resistance to Leptin?" J. Clin. Endocrinol. Metab. **87**(3), 1184–1188 (2002).
31. U. Lotze, H. Lemm, A. Heyer, and K. Müller, "Combined determination of highly sensitive troponin T and copeptin for early exclusion of acute myocardial infarction: first experience in an emergency department of a general hospital," Vasc. Health Risk Manag. **7**, 509–515 (2011).
32. D. Chan and L. L. Ng, "Biomarkers in acute myocardial infarction," BMC Med. **8**(1), 34 (2010).
33. T. Zeller, M. Hughes, T. Tuovinen, A. Schillert, A. Conrads-Frank, H. Ruijter, R. B. Schnabel, F. Kee, V. Salomaa, U. Siebert, B. Thorand, A. Ziegler, H. Breek, G. Pasterkamp, K. Kuulasmaa, W. Koenig, and S. Blankenberg, "BiomarCaRE: rationale and design of the European BiomarCaRE project including 300,000 participants from 13 European countries," Eur. J. Epidemiol. **29**(10), 777–790 (2014).
34. C. Nicolaou, W. T. Lau, R. Gad, H. Akhavan, R. Schilling, and O. Levi, "Enhanced detection limit by dark mode perturbation in 2D photonic crystal slab refractive index sensors," Opt. Express **21**(25), 31698–31712 (2013).
35. M. Pisco, A. Ricciardi, I. Gallina, G. Castaldi, S. Campopiano, A. Cutolo, A. Cusano, and V. Galdi, "Tuning efficiency and sensitivity of guided resonances in photonic crystals and quasi-crystals: a comparative study," Opt. Express **18**(16), 17280–17293 (2010).

#246022 Received 14 Jul 2015; revised 14 Aug 2015; accepted 14 Aug 2015; published 1 Sep 2015

1. Introduction

Early recognition and treatment have an important influence on the course of diseases, both for acute cases as the exclusion of myocardial infarction [1] as well as for slowly progressing diseases such as diabetes type 2 [2]. Therefore, compact, fast operating, decentralized, and easy-to-use sensors are of high interest for point-of-care applications. These sensors should be able to validate multiple and specific biomarkers for non-ambiguous diagnostics and patient-specific therapy. Various point-of-care devices have been developed to meet these demands [3–5]. The most widespread approaches are label-based detection schemes such as fluorescence assays [6]. They have the disadvantage of the need to use additional reagents and preparation steps [7]. In comparison, label-free biosensing approaches are able to detect specific biomarkers directly and in real-time without additional preparation [8]. Typically, these biosensors consist of a selective and specific biological recognition component (receptor) directly connected to a transducer [9]. The transducer transforms the binding kinetics of the target biomarkers into a signal detectable with, e.g., optical read-out systems [10, 11]. The selection of optical signal transducers ranges from waveguide interferometers [7, 12] over surface plasmon resonance sensors [11, 13] to microcavity sensors [14] and photonic crystal sensors [15–18]. With photonic crystal slabs (PCS) as transducers specific, cost-efficient and compact systems may be realized. PCS are waveguides with a periodic nanostructure in a high refractive index material as depicted in Fig. 1(a). They support quasi-guided modes that are visible as guided-mode resonances (GMRs) in the optical spectrum and can be excited in transmission as well as in reflection. Because of the evanescent fraction of the quasi-guided modes propagating above the PCS surface, refractive index changes Δn on the PCS surface result in a wavelength shift $\Delta\lambda$ of the GMRs as shown schematically in Fig. 1(b). This effect can be used by functionalizing the PCS surface with receptors such as antibodies or aptamers, which recognize the target and bind it to the receptor on the PCS surface.

In several previous works the functionality of this principle was demonstrated by tracking the shift of the GMR wavelength $\Delta\lambda$ during biomarker detection with a spectrometer [16, 18]. For compact point-of-care systems miniaturization of the spectrometer setup [19] as well as a smartphone adapter and use of the smartphone camera [20] have been investigated. For multiplexed detection of a biomarker array, a compact spectrometer-free setup is preferable. Recently, a handheld plasmonic biosensor was presented employing lens-free evaluation of diffraction patterns comparing samples before and after functionalization [21]. We have previously introduced a compact photometric measurement system tracking an intensity change ΔI upon binding of biomarkers to the surface. For a decrease of the refractive index contrast between waveguide material and substance on the surface, the quality factor Q of the GMR increases corresponding to a lower resonance width [22, 23]. For a PCS with material losses, a higher quality factor also reduces the resonance peak intensity I_{peak} due to the longer interaction time with the lossy PCS [23, 24]. Both effects result in a reduced integrated resonance intensity observable in an intensity measurement. Additionally, we design the optical transmission system such that the system response also decreases with wavelength. Thus, a further reduction in intensity with wavelength change is obtained [25]. We here introduce a spectrometer-free handheld biosensor system based on imaging of the integrated intensity change ΔI for binding of biomolecules to a photonic crystal sensor surface. Integrating the photonic crystal sensor surface into a disposable microfluidic chip with filter unit [26] potentially allows for multiparametric biomarker detection in human blood for point-of-care applications. By spotting of specific binding sites for different types of molecules and imaging read out, a geometry-multiplexed detection scheme is realized as schematically shown in Fig. 1(c). Here, we demonstrate the multiplexed, label-free measurement of binding kinetics for both antibody- and aptamer-functionalized photonic crystal surfaces with a simple CMOS camera.

#246022 Received 14 Jul 2015; revised 14 Aug 2015; accepted 14 Aug 2015; published 1 Sep 2015

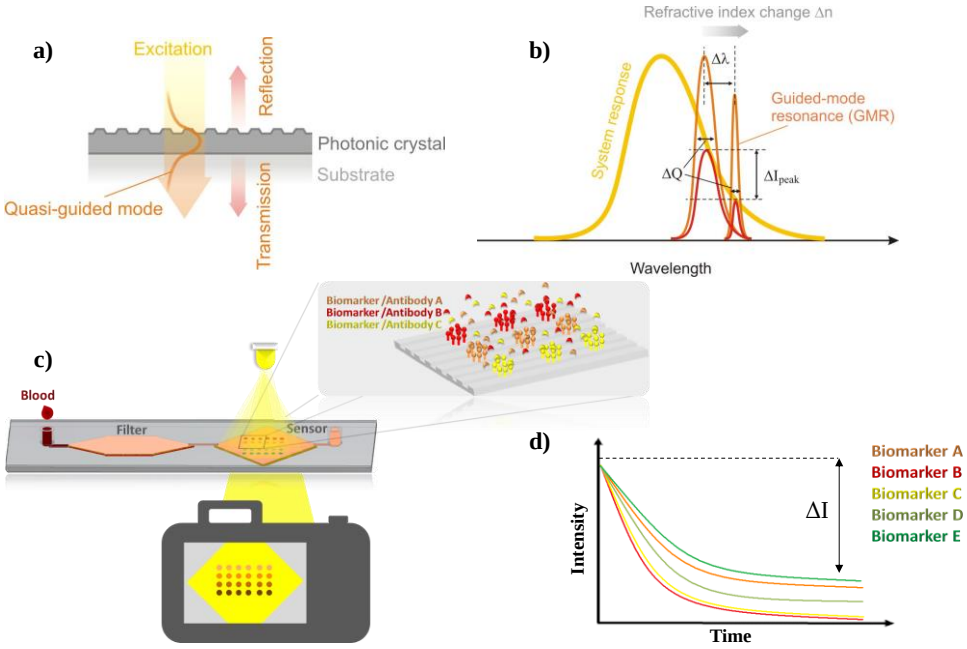

Fig. 1. Vision of a disposable microfluidic test chip for label-free and parallel detection of multiple biomarkers with a compact optical imaging system. (a) Schematic of photonic crystal slab (PCS). Incident light is coupled into quasi-guided modes and scattered light is observed as guided mode resonances (GMRs) in transmission and reflection. (b) GMRs in the transmission spectrum experience a change in wavelength $\Delta\lambda$ for a refractive index change Δn due to biomarker binding. They also incur a reduction of quality factor Q and maximum intensity. With a wavelength-dependent optical system response, this is translated into a peak intensity change ΔI_{peak} and thus an integrated intensity change ΔI on the camera. (c) Schematic of microfluidic chip with nanostructured and spot-wise functionalized sensor field. (d) Schematic of intensity signals at different positions for biomarker binding. In this publication, the fabrication and functionalization of the sensor surface, the camera measurement setup and the evaluation algorithms, as well as measurements of time-resolved multiplexed binding of different biomarkers are presented. The microfluidic chip is described in [26].

In section 2 the fabrication of the nanostructured transducer surface and the procedure for specific bio-functionalization are described. In section 3 the functionality principle of the developed read-out system as well as the evaluation algorithm for reducing drift are explained. Experimental results for simultaneous and specific detection of multiple biomarkers are presented in section 4. By continuously taking photographs of the PCS surface local intensity changes are observed dependent on the ligands´ position. Conclusions are drawn in section 5.

2. Fabrication of biosensor

The fabrication of the biosensor consists of three parts. First, a polydimethylsiloxane (PDMS) secondary stamp is fabricated from a glass master. Second, the photonic crystal slabs (PCS) are realized by ultraviolet (UV) nanoimprint lithography. Third, the PCS are biofunctionalized. These three fabrication parts are described in the next three sections.

2.1 Fabrication of secondary PDMS stamp

A glass master with a grating period of Λ = 370 nm, a structure depth of t = 60 nm and a duty cycle of 40:60 is employed. This glass master is replicated into a more flexible PDMS secondary stamp. The flexibility of the secondary stamp prevents problems with incomplete replication over the2.5 x 2.5 cm^2 sensor surface, which we experienced for direct replication of the glass master. For the secondary PDMS stamp Sylgard 184 and curing agent (both from

#246022 Received 14 Jul 2015; revised 14 Aug 2015; accepted 14 Aug 2015; published 1 Sep 2015

DOW Corning) are mixed in a ratio of 8:1 for 15 minutes in a mixing tube (*IKA*). The glass master is placed into a teflon adapter and PDMS is poured over the master. Afterwards, it is evacuated for 15 minutes inside a vacuum chamber to remove air bubbles from the PDMS. Then, the PDMS is cured in an oven at 130°C for 20 minutes. Finally, the cured PDMS secondary stamp is cut from the teflon adapter and pulled off the glass master.

2.2 Fabrication of photonic crystal slab

For PCS fabrication 25 x 25 mm^2 glass substrates with a thickness of 1 mm are cleaned with acetone and isopropanol for 15 minutes each in an ultra sonic bath. After dehydration for 10 minutes at 160°C on a hotplate the surface of the glass substrates is activated with oxygen plasma for 2 minutes with an RF power of 200 W (*Sentech SI 100*) to enhance the adhesion of the adhesion promoter and thus of the photoresist. The following fabrication of the PCS is depicted in Fig. 2. 150 µl adhesion promoter (Amoprime, *AMO GmbH*) are spin coated for 30 seconds at 3000 rpm onto the substrate. The substrates are baked on a hotplate for 2 minutes at 115°C and cooled for another 2 minutes. Next 150 µl photoresist (Amonil, *AMO GmbH*) is spin coated on top with the same parameters to generate a 200 nm thick layer. During the warm-up time of the UV halogen lamp the PDMS secondary stamp is pressed carefully into the resist to transfer the nanostructure from the stamp onto the substrate. The substrate including the stamp on top is exposed for 80 seconds to the UV lamp to harden the photoresist. After the PDMS secondary stamp is pulled off the substrate, a 70-nm thick titanium dioxide layer is deposited on top by reactive sputtering.

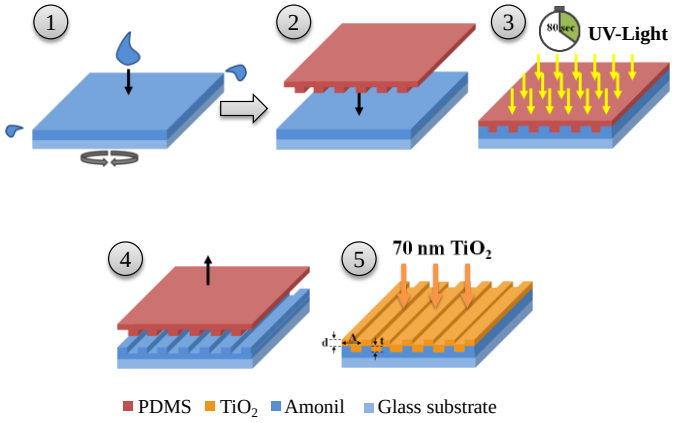

Fig. 2. Photonic crystal fabrication steps. For transferring the linear grating from a PDMS stamp onto a glass substrate UV soft nanoimprint lithography is used and subsequently a 70-nm titanium dioxide layer is deposited on top by reactive sputtering.

2.3 Fabrication of biosensor

To convert the PCS into a biosensor the PCS surface is first enriched with hydroxy groups by treatment with oxygen plasma for 5 minutes and 50 W (*Sentech* SI 100). Next the sample is transferred into a nitrogen-filled glovebox. Here, it is cleaned in dry ethyl alcohol (9065.3, *Carl Roth*) and in dry methyl alcohol (322415, *Sigma Aldrich*) each for 5 minutes. Afterwards, the PCS is incubated for 1 hour in a solution of 260 µl (3-aminopropyl)triethoxysilane (APTES) (281778, *Sigma Aldrich*) dissolved in 24.5 ml dry methyl alcohol at room temperature to silanize the complete titanium dioxide surface. The resulting molecule after this silanisation step is given in Fig. 3(a1).

Subsequently, the substrate is thoroughly washed with methyl alcohol and baked for 20 minutes on a hotplate at 110°C. 1,4-phenylene diisothiocyanate (PDC) (258555, Sigma Aldrich) is used as crosslinker to immobilise any ligand modified with an amine on the sensor surface. 100 mg PDC are dissolved in a solution of 500 µl pyridine (494410, Sigma Aldrich)

#246022 Received 14 Jul 2015; revised 14 Aug 2015; accepted 14 Aug 2015; published 1 Sep 2015

and 4.5 ml N,N-dimethylformamide (DMF) (227056, Sigma Aldrich). The sample is incubated for 2 hours in this solution at room temperature. The sample is washed again with methyl alcohol. The resulting molecule is shown in Fig. 3(a2).

For covalent coupling of immobilised proteins (different ligands) the sample is removed from nitrogen atmosphere and placed in a humidity chamber. Now 1.00 µM of different ligands dissolved in sodium acetate buffer (pH 4.5) (176-2121, Bio-Rad Laboratories GmbH) are placed in 500 nl drops with a pipette on the PCS surface and are incubated over night in the humidity chamber. After 24 hours, the non-bound ligands are washed off with Dulbecco's phosphate buffered saline (pH 7.4) (DPBS) (14190-169, Lifetechnologies GmbH).

For passivation of the remaining functional groups first 1.00 M ethanolamine HCl (176-2450, Bio-Rad Laboratories GmbH) and then 1.00 mg/ml bovine serum albumin (BSA) (05470, Sigma Aldrich) dissolved in DPBS cover the sample surface for 30 minutes, each. After each passivation step the surface is washed with DPBS. In Fig. 3(a) schematic representations of the resulting molecules for these last two functionalization steps are shown.

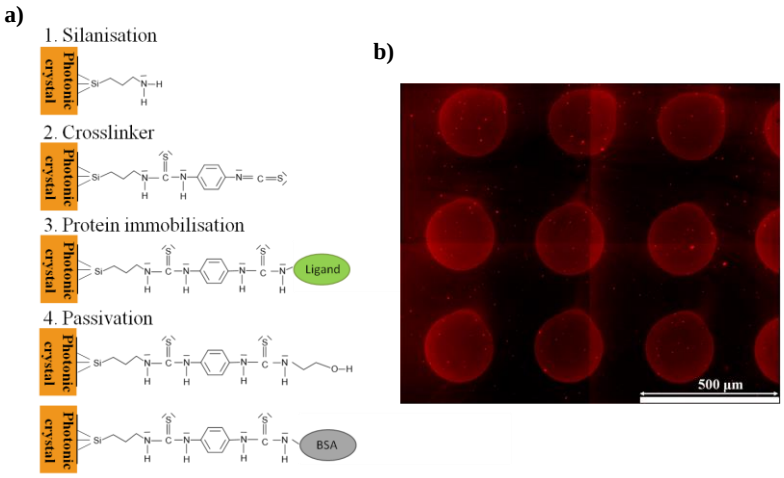

Fig. 3. a) Schematic of the resulting molecules after each functionalization step. b) Evaluation of local functionalization by spotting fluorescence dye ATTO594 modified with amine on sensor surface instead of ligand. Resulting fluorescence photographs are shown.

To verify the process of local functionalization the fluorescence dye (ATTO594, *ATTO-TECH GmbH*) modified with an amino group is coupled covalently instead of a ligand (Fig. 3(a) step 3) to the sensor surface by spotting 500 pl drops of 100 µM ATTO594 dissolved in deionized water. Under a fluorescence microscope the locally immobilized ATTO594 is clearly visible as well-defined, red-fluorescent spots with a size of about 250 µm (Fig. 3(b)). The red fluorescent speckles belong to pollutions and are also visible in the normal bright field image.

3. Measurement system

3.1. Functional principle and setup

For the measurements presented here, the sensor is placed within a fluid cell as depicted in Fig. 4. An o-ring is placed between the 25 x 25 mm^2 large sensor and a glass substrate. Two butterfly cannulas are pierced through the o-ring for analyte exchange and all is fixed with two screwed substrate holders. The fluid cell is then positioned between two crossed linear polarization filters and between a parallelizing and a focusing optics. Because of this arrangement only the fraction of the GMRs coupling out of the PCS passes the second polarization filter and reaches the camera sensor, while nearly all excitation light is suppressed [25]. A colored light emitting diode (LED) with a narrow-band spectrum and steeply falling edges is used as excitation source (LY T686-Q2T1-26, *OSRAM Opto*

#246022 Received 14 Jul 2015; revised 14 Aug 2015; accepted 14 Aug 2015; published 1 Sep 2015

Semiconductors). The spatially-resolved transmission intensity is recorded with a CMOS camera sensor (DCC1645C, *Thorlabs GmbH*). Via a USB-interface the LED as well as the camera are connected to a computer. Here, only the green color channel of the camera is read out with a *LabVIEW* program. The LED spectrum and the camera sensitivity in the green color channel are shown in Fig. 4(c). In the GMR spectrum in Fig. 4(c) the broader and higher-intensity TE resonance is visible at around 670 nm. Here, the TM resonance at 600 nm is employed. With the wavelength of the TM GMR aligned to the falling edge of the LED spectrum and the camera sensitivity in the green color channel, the resonance shift due to biomarker binding events is converted into an intensity reduction. The PCS is placed for normal incidence transmission in the measurement setup. No angle alignment is used. We find that the angular alignment is not critical as the system response is significantly broader than the resonance in our setup. The measurement procedure works reliably as long as the GMR coincides with the falling edge of the system response. A different initial value is detected by reference to the non-functionalized surface areas on the PCS. Figure 4(d) shows a photograph of the realized measurement setup with an overall size of 13 cm x 3.5 cm x 4.9 cm.

For protein detection the molecular solution under study is injected into the fluid cell with a syringe pushing the replaced fluid into the beaker seen in Fig. 4(d). Preliminary experiments showed that for an injection of 5 ml a complete fluid exchange is obtained. The camera takes one image of the sensor surface every 0.5 seconds. With the *LabVIEW* program real-time and variably adjustable pixel binning is possible and the median for each pixel over a variable number of images can be calculated to reduce background noise. For the following protein detections binning over 8 x 8 pixels and the median over five images are chosen, whereby one intensity image matrix with 200 x 150 elements is saved every 2.5 seconds in a text file for data post processing. With the total image size corresponding to a measurement field size of 20 x 15 mm^2, this corresponds to a spatial resolution of 100 µm.

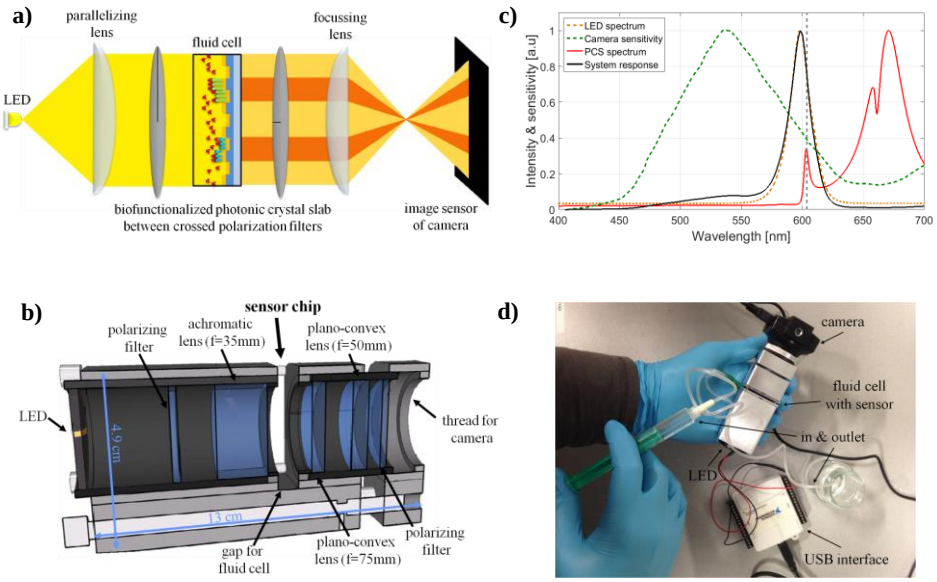

Fig. 4. a) Schematic of imaging read-out system. The darker (red) light cones symbolize a reduced intensity on the camera compared to the brighter (orange) background. b) Computer aided 3D design of the photometric read-out system. c) LED spectrum, camera sensitivity, product of LED spectrum and camera sensitivity, and PCS spectrum with crossed polarization filters. d) Photograph of photometric read-out system with camera, LED, and optics within the metallic torso, the fluid cell with the biosensor, the butterfly cannula for in and outlet and the USB-interface.

We investigate the response of our imaging read-out system on refractive index changes by performing refractometric measurements with the above mentioned parameters. A non-

#246022 Received 14 Jul 2015; revised 14 Aug 2015; accepted 14 Aug 2015; published 1 Sep 2015

functionalized PCS caps the fluid cell, which is filled initially with distilled water. As depicted in Fig. 5, replacing the distilled water with a solution of 20% isopropanol and 80% distilled water the surrounding refractive index in the fluid cell increases from n_{H2O} = 1.33 to $n_{20\%iso}$ = 1.34. This causes an integrated intensity reduction (ΔI = 9.6%) of the transmitted light. After another five minutes distilled water is filled again in the fluid cell and the intensity increases to the origin level.

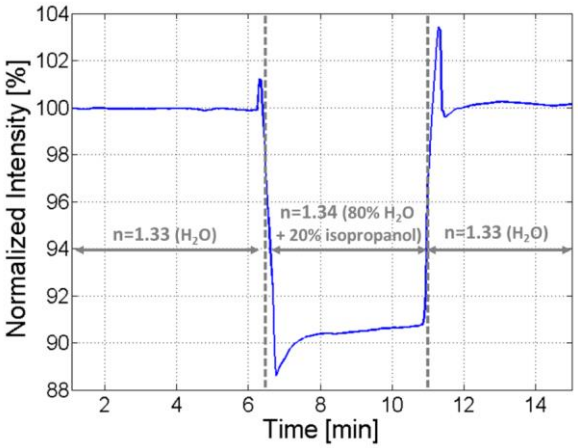

Fig. 5. Refractometric measurement with analyte change from distilled water to 20% isopropanol and 80% distilled water. The median of the intensity values over the entire image and thus over the sensor is calculated and the resulting values normalized to the first value are plotted over time

3.2. Evaluation algorithms

The limit of detection (LOD) in wavelength- or angle-based detection methods, where a spectrometer is required, is mostly a function of the resonance width and the sensitivity of the resonance. The LOD in intensity-based detection, as applied in this paper, however, is a function of the system noise and drift. More importantly, any parasitic intensity fluctuation, which can occur due to dirt contamination of the liquid or unwanted reflection in the optical system, is also limiting the LOD. Therefore, a pure intensity-based measurement is less robust than the wavelength- or angle-based detection methods. Here, we apply an imaging intensity based scheme, where we use the non-functionalized areas of the sensor as reference and cancel out the intensity fluctuations and system drift.

To generate first a signal sequence from the measured intensity images an algorithm is implemented with the program *MATLAB*. An element-wise subtraction of the intensity matrix at the first point in time from the last one is performed. In the resulting false-color difference image the biomarker association dependent on the ligands´ positions becomes visible as local and drop-shaped intensity reductions (Fig. 6(a)).

#246022 Received 14 Jul 2015; revised 14 Aug 2015; accepted 14 Aug 2015; published 1 Sep 2015

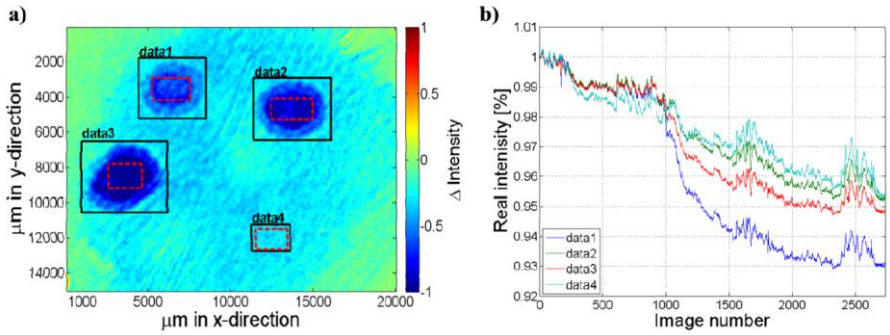

Fig. 6. a) False-color difference intensity map obtained by element-wise subtraction of the first intensity image matrix from the last one. The three measurement fields and one reference field are marked by red dashed rectangles. b) The median of the intensity over all positions within the equivalent fields is calculated and the resulting values normalized to the first value are plotted against the image number, which correlates to measurement time.

Plotting the median over all intensities within the measurement and reference fields normalized to the first intensity value (red rectangles in Fig. 6(a)), no typical association curves can be identified in the resulting graph (Fig. 6(b)). The whole system and especially the intensity of the LED cause a position-dependent drift. This drift can be temperature drift of the sensor and electric components or angular drift of the sensor, which also results in an intensity drift.

An image processing algorithm is employed to eliminate drift. The non-functionalized areas around the measurement fields are only affected by the background drift and not by binding events. Therefore, these areas are predestinated for drift estimation. First, the measurement fields are cut out of the image (black rectangle). Next, these areas are interpolated by using the natural neighbor interpolation. Comparing the raw image (Fig. 7(a)) with the image with the interpolated areas (Fig. 7(b)) the interpolation leads to reasonably fitted results.

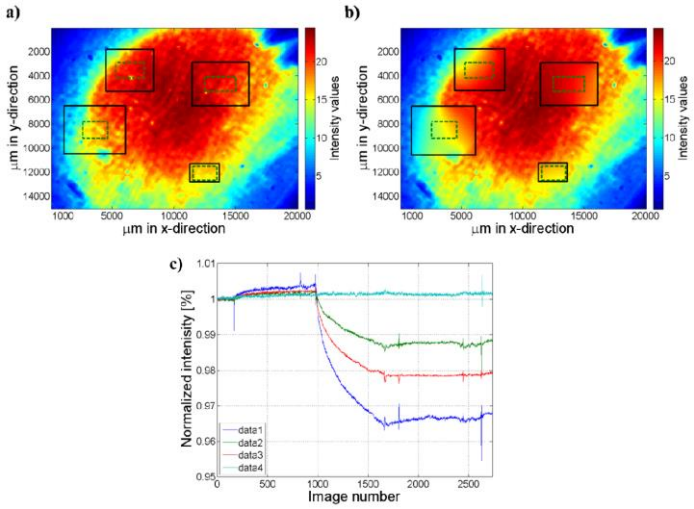

Fig. 7. a) Raw false-color image of the sensor surface with the corresponding distribution of the transmitted light and the markers for the measurement fields. b) The same intensity image with the estimated background obtained by interpolating the surrounding areas. c) After drift compensation the median intensity over all intensity matrix elements within the measurement fields is calculated and the normalized intensities are plotted against the number of images correlated to the time.

#246022 Received 14 Jul 2015; revised 14 Aug 2015; accepted 14 Aug 2015; published 1 Sep 2015

Dividing the raw image by the interpolated one and calculating the median over all intensities within the green rectangles, the association of the biomarkers to the sensor surface is obtained as depicted in Fig. 7(c). The normalized intensity of the reference field (data 4) exhibits a straight course of intensity over time with only low noise, while no binding events and nearly no drift effects are observed.

4. Results of multiparametric protein detection

4.1 Detection with antibodies

For multiplexed protein detection six measurement areas were functionalized with three types of receptors. The following receptors are immobilized after drop-wise application to the surface of the photonic crystal: two 500-nl drops of 1.00-µM recombinant human CD40 ligand (AF-310-02-B, *PeptroTech GmbH*), three 500-nl drops of 1.00-µM recombinant human EGF (CS-C1020, *CellSystems*) and one 500-nl drop of 1.00-µM biotinylated bovine serum albumin (BSA-biotin) (A8549-10MG, *Sigma Aldrich*) all dissolved in sodium acetate buffer. An experimental sequence with the successive addition of the three different types of proteins is conducted in order to demonstrate the specific binding. In Fig. 8 the resulting normalized intensities within the six measurement fields and one reference field are plotted against time. Additionally, the resulting difference images are shown to demonstrate the local intensity reduction only dependent on the specific ligand's position. At the beginning of the experiment pure DPBS is filled into the fluid cell to generate a baseline signal. After ten minutes the buffer is replaced by the first protein buffer solution consisting of 90.0 nM (13.5 µg/ml) CD40 ligand antibody (500-P142G-B, *PeproTech GmbH*) dissolved in DPBS. During the incubation time of 40 minutes the association of the CD40 ligand antibody causes an intensity reduction of up to ΔI_{max} = 4.3% in the corresponding functionalized areas only. Other measurement fields do not show any unspecific binding events. By washing with pure DPBS the non-bound antibody is removed, the intensity decrease stops and the signal is stable over the remaining detection time. After another 10 minutes the second protein solution with 90.0 nM (13.5 µg/ml) EGF antibody (500-P45-B, *PeproTech GmbH*) is filled into the fluid cell. After another 40 minutes the EGF antibody association is only visible in the signal sequence for the three specific measurement fields (ΔI_{max} = 2.7%). Next, the protein solution is replaced by pure buffer. Finally, the incubation of 500 nM (30 µg/ml) streptavidin (S4762-1MG, *Sigma Aldrich*) buffer solution is observed in the intensity of the last ligand position (ΔI_{max} = 1.9%). The non-bound streptavidin is removed with pure buffer.

Figure 8 clearly demonstrates the specific multiplexed detection of proteins. For the same protein different signal amplitudes are observed on different measurement fields. Maybe this can be attributed to the much higher ligand concentration on the sensor surface compared to the protein concentration in solution and imperfect mixing. Another possibility is variances in the functionalization process as functionalized areas, which seem to have different sizes. Further work is required to obtain reproducibility in the functionalization. The signal amplitudes for the binding of CD40 ligand antibody and of EGF antibody are expected to be similar, because of the same concentration and the same molecular weight (150 kDa).

We calculate a limit of detection (LOD) of around 166 pM (24 ng/ml) considering the signal sequence with the maximum intensity reduction. The LOD is defined as $LOD = (3 \times \sigma / \Delta I_{max}) \times c$ with σ as the standard deviation of the baseline signal, ΔI_{max} as the intensity difference and c as the protein concentration in this case of the CD40 ligand antibody.

#246022 Received 14 Jul 2015; revised 14 Aug 2015; accepted 14 Aug 2015; published 1 Sep 2015

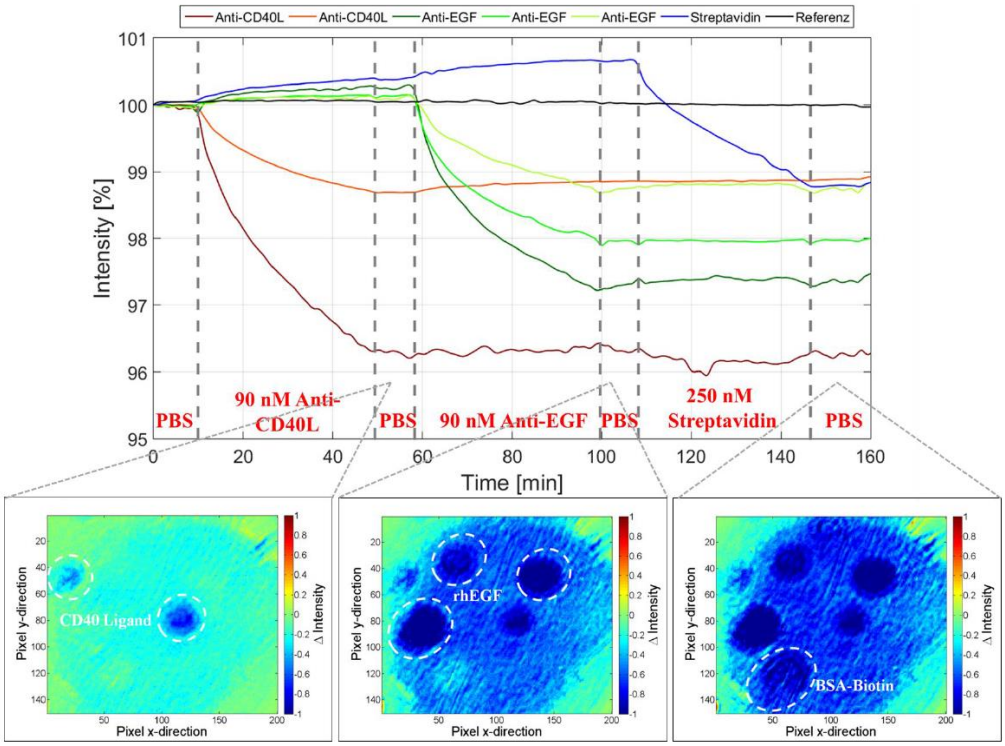

Fig. 8. The association of first 90.0 nM CD40 ligand antibodies (150 kDa), second 90.0 nM EGF antibodies (150 kDa) and third 500 nM streptavidin (60 kDa) all dissolved in DPBS is observed in the normalized intensities of the transmitted light, while no unspecific binding events are visible in the signal sequence.

4.2 Detection with aptamers

In a second experiment we investigate the use of aptamers as capture molecules. Aptamers are synthetically produced binding molecules. They offer low temperature sensitivity, are highly specific to the detection molecule, and can be produced with a high reproducibility [23]. We choose thrombin as the detection protein and functionalize the photonic crystal surface with two types of thrombin binding aptamers. One has only one spacer between the amino group and the actual aptamer (oligo sequence: 5′-C6-Aminolink-XAG TCC GTG GTA GGG CAG GTT GGG GTG ACT-3′ with X = Spacer-HEG/PEO, *metabion international AG*) (NH_2-HEG-HD22) the second one has two spacers in between (oligo sequence: 5′-C6-Aminolink-XXA GTC CGT GGT AGG GCA GGT TGG GACT-3′ [27] with X = Spacer-HEG/PEO, *metabion international AG*) (NH_2-2xHEG-HD22). Figure 9 shows the experimental results of two measurement cycles of association, dissociation, and regeneration. In this case tris-HCl-buffer (154563-100G, *Sigma Aldrich*, 9280.3, *Carl Roth GmbH + Co. KG*) (pH 7.4) is used for baseline generation and for dissolving 250 nM human alpha thrombin (HCT-0020, *CellSystems*). During the association phase the Aptamer with the shorter spacer provides a higher intensity reduction by $\Delta I = 0.1\%$. This may be attributed to the evanescent fraction of the guided modes. The electric field strength of the guided modes decreases with the distance to the sensor surface. Therefore, a lower signal is expected for binding further away from the surface. When washing with pure buffer after the association phase, the intensity increases slightly. This may correspond to dissociation of part of the proteins. This effect was not observed for experiments with antibodies in Fig. 8. Aptamers bind the specific target protein according to the key-lock principle and thus docking to the protein via their 3D structure. In our case the aptamer binding seems to have a lower stability than the protein-antibody

#246022 Received 14 Jul 2015; revised 14 Aug 2015; accepted 14 Aug 2015; published 1 Sep 2015

binding. Additionally, the aptamers are sensitive to the environmental pH level. This is used to regenerate the sensor by washing with a slightly acidic tris-HCl-buffer (pH 5.0). The acid environment causes a different folding of the aptamer structure and thus a complete dissociation of the bound thrombin. The procedure of association, dissociation, and regeneration is repeated with nearly the same results.

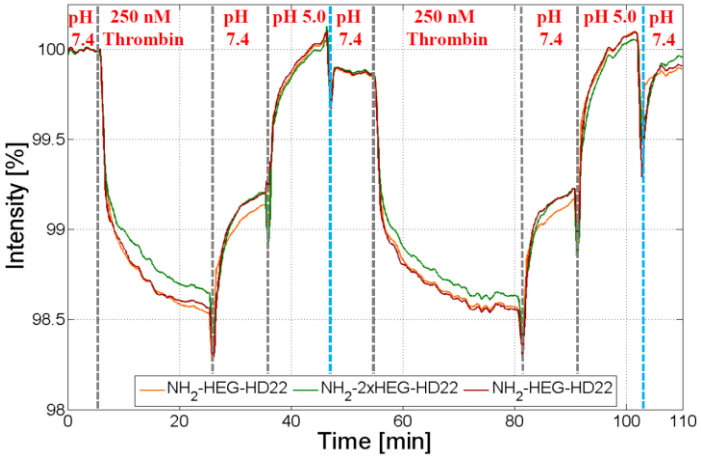

Fig. 9. The association, dissociation, and regeneration of 250 nM thrombin (36.7 kDa) dissolved in tris-HCl-buffer (pH 7.4) can be observed in the normalized intensities of the transmitted light. The signal amplitude for the shorter ligand is higher than the one for a longer ligand.

Figure 10 summarizes the response of the biosensor to each detected protein and gives an overview of the statistical distribution. The intensity amplitudes for the thrombin detection exhibit a lower standard deviation and thus a higher reproducibility compared to the other measurements. This may be explained with the higher chemical stability of the thrombin binding aptamers compared to BSA-biotin, streptavidin, CD40 ligand, EGF and their antibodies [28].

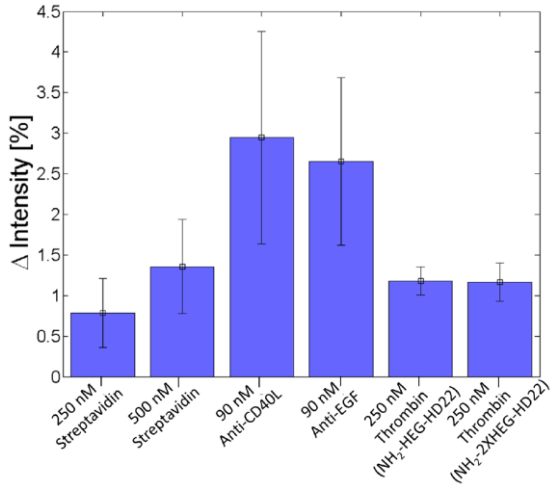

Fig. 10. Bar diagram reflecting the median and the standard deviation over all resulting signal amplitudes for each protein detection performed with the handheld, spectrometer-free biosensor. In the statistics 12 data sets are included for 250 nM streptavidin, 3 data sets for 500 nM streptavidin, data sets for CD40L, 5 data sets for Anti-EGF, 8 data sets for Thrombin (1 Spacer), and 2 data sets for Thrombin (2 Spacer).

#246022 Received 14 Jul 2015; revised 14 Aug 2015; accepted 14 Aug 2015; published 1 Sep 2015

7. Conclusion

We demonstrated the simultaneous, label-free and specific detection of the three biomarkers CD40 ligand, EGF and streptavidin with a handheld, spectrometer-free imaging biosensor system. Image processing was successfully employed to reduce drift by calibration to non-functionalized surface areas. Additionally, we performed experiments with thrombin-binding aptamers and obtained better reproducibility compared to the antibody experiments. These first proof-of-principle experiments used higher protein concentrations than are typically found in life sciences. But considering the LOD obtained here, there is a big potential for achieving more life science related concentrations.

The sensing chamber of the microfluidic chip depicted in Fig. 1(c) [26] is 100 µm high and requires 15 µl of serum for filling. This is obtained from 40 µl of whole blood demonstrating that a single drop of blood is sufficient for filling the chamber. On the 1-cm^2 sensor surface it is feasible to place 20 x 20 = 400 functionalized spots with 12 nl drops, an approximate spot diameter of 350 µm, and a pitch of 500 µm. This corresponds to a surface coverage of around 40% leaving enough surface space for referencing. This high number of spots shows that a whole panel of biomarkers may be tested in parallel with multiple spots for one biomarker for improved sensitivity. Even higher numbers of spots may be possible for a different functionalization scheme. Ultimately, the spatial resolution of the method is limited by the propagation length of the quasi-guided modes, which is in the µm-range as seen by comparison to AFM-images in [23]. An important advantage of the method is the single-shot imaging approach that does not require scanning. This allows for reliable identification of measurement fields and reference areas by placement of simple alignment markers for image processing. The speed of detection is limited by the binding kinetics of the biomarkers and in the range of minutes for monitoring the kinetics.

For a diagnostic tool sensitivities for target proteins in the pg/ml to mg/ml range are necessary. For example, diabetes markers have levels of Adiponectin: µg/ml [29]; ApoB: mg/ml [29]; CRP: µg/ml [29]; Ferritin: ng/ml [29]; IL-1 RA: pg/ml [30]. Typical cardiac marker concentrations of interest are Troponin I: 40 pg/ml [1]; CK-MB: 6 ng/ml [1]; Myoglobin: 200 ng/ml [1]; Tropnin T: 14 pg/ml [31]; Copeptin: 14 pmol/ml (56 pg/ml) [31]. The search for relevant cardiac markers to predict cardiovascular risk is a current topic of research [32, 33]. It is expected that larger panels of relevant markers will be found and need to be tested in parallel. Also, for reliable diagnosis, several specific testing times of, for example, immediately, 1 hour, and 4 hours after symptoms appear are optimal. On this time frame, point-of-care testing is crucial. Currently, only single biomarker tests are available with a sensitivity of 1 ng/ml such as the test strip meditrol® Troponin I Test from *medichem Vertriebs GmbH*. Our estimated limit of detection of 24 ng/ml is still 24 times worse in terms of sensitivity. It already is in the range that is interesting for some of the diabetes markers as well as some cardiac markers. Further improvement of the sensitivity is highly desirable to allow for a larger panel of biomarkers. Next we will continue with the following two steps for improving the sensitivity of our sensor. First, well will employ a PCS with a higher sensitivity obtained with multiperiodic or aperiodic nanostructures [34, 35]. Second, we will use smaller functionalized spots for higher concentration of bound biomarkers and thus larger local intensity changes. Overall, this approach is promising for a multiplexed, compact and highly specific biosensor attractive for future point-of-care applications.

Acknowledgments

The authors acknowledge support by the European Research Council within the project Photosmart (307800) and by the German Federal Ministry of Education and Research (BMBF) within the project BioCard (0316145A & B).

#246022 Received 14 Jul 2015; revised 14 Aug 2015; accepted 14 Aug 2015; published 1 Sep 2015